JOURNAL OF PROPULSION AND POWER
Vol. 22, No. 2, March–April 2006

Experiments on Scramjet Engine with Ramp-Compression Inlet at Mach 8

Tetsuo Hiraiwa*
Japan Aerospace Exploration Agency, Tsukuba Space Center, Ibaraki 305-8505, Japan
and
Takeshi Kanda,† Kan Kobayashi,‡ and Toshihito Saito§
Japan Aerospace Exploration Agency, Kakuda Space Propulsion Center, Miyagi 981-1525, Japan

A recent modification to our scramjet engine and its experimental achievements under Mach 8 flight condition is presented. This modified engine has a ramp block, which covers its entire top wall, instead of the strut of the original engine. This block suppressed the inlet–combustor interaction under a large adverse pressure gradient and enlarged the inlet starting condition, compared with conditions of the engine with the strut-compression system. With this wider starting condition, the modified model produced positive net thrust, namely, larger thrust than its own drag. This engine did not go into the unstarted condition nor lose its thrust abruptly, because the airflow on the inlet ramp block separated gradually from its downstream end with an increase of the combustor pressure.

Nomenclature

D_{cowl}	=	drag on outer surface of cowl
D_{int}	=	engine drag from internal duct under no-fueled condition
D_{net}	=	net drag, $D_{\text{int}} + D_{\text{cowl}}$
F_{net}	=	net thrust, $\Delta F - D_{\text{net}}$
F_{xa}	=	axial force under no-fueled condition, measured by force measurement system
F_{xc}	=	axial force under fueled condition, measured by force measurement system
$\dot{m}_{\text{fuel}}$	=	fuel mass flow rate
P_s	=	static pressure of airflow at exit of facility nozzle
P_w	=	static pressure on engine walls
x	=	streamwise distance from leading edge of top wall
ΔF	=	thrust increment due to fueling, $F_{xc} - F_{xa}$
ϕ	=	fuel equivalence ratio

I. Introduction

THE scramjet, the dual-mode ramjet, and combined-cycle engines are key candidates for employment in the envisioned transatmospheric, hypersonic vehicle that will realize a more economical transportation system to Earth orbit. Recently, the X-43 flew successfully powered by scramjet engines at Mach 7 and 10 (Ref. 1). The combined propulsion research group of the Japan Aerospace Exploration Agency, formerly part of the National Aerospace Laboratory of Japan, has been testing two subscale scramjet engine models, E1 and E2, under the Mach 8 flight condition since 1995. These tests have been conducted at the Ramjet Engine Test Facility of Kakuda Space Propulsion Center, which is a freejet, blowdown-type wind tunnel specialized for scramjet and ramjet engines. This wind tunnel can simulate Mach 4, 6, and 8 flight conditions with 2-m-long engine models. Details of the tunnel and previous test results are summarized in Ref. 2.

These models successfully produced positive net thrust under flight conditions of Mach 4 and 6 (Ref. 2). For tests under the Mach 8 flight condition, the E1 model was modified by replacement of its strut and an increase of its contraction ratio to 8.3 (Ref. 3). This modified E1 model attained high combustion efficiency. However, it could not produce positive thrust due to the large base drag of the strut and to a drift of the primary combustion area from the combustor to the nozzle section. Furthermore, when the combustion occurred and local pressure at the combustor section increased, the model easily went into the unstarted condition, because flow separation on the top wall moved upstream from the combustor section to the inlet. To improve combustion efficiency, the E1 engine was modified again, with a short ramp block in the inlet to combustor section, in addition to the original strut.[4] This model, designated E1SR here, was also designed to conduct preliminary tests for a movable configuration and ramp-compression-system engine. The overall contraction ratio of the E1SR became 9.3. The operable equivalence ratio of this model was larger under the started condition. Moreover, it attained combustion primarily at the designed location around the fuel injectors and high combustion efficiency due to suppression of separation on the top wall. However, the E1SR could not produce sufficient thrust due to an unsuitable configuration in the divergent section, that is, a steep downstream base configuration of the temporary ramp block.

To produce more thrust under the Mach 8 flight condition, another engine model, designated E2, was designed.[5] As in the E1, this model incorporated the sidewall compression and expansion system. Except in its inlet section, this engine had no sweptback angle on the sidewalls to prevent distortion in the airflow and combustion gas flow. The model had an isolator section longer than the E1, especially for its top wall side. This longer isolator was expected to tolerate a great adverse pressure gradient that appeared in the inlet and combustor section. Though the isolator extended the starting limit and increased the thrust, the modifications could not produce thrust sufficient to overcome the engine drag. The insufficient thrust production was caused by insufficient sustenance for the adverse pressure gradient in the inlet to combustor section and insufficient air capture in the inlet.

Based on the successful results on combustion conditions and startability of the E1SR, we modified the E2 model by attaching a ramp block and removing the strut. This model is named E2R in this paper. We first introduce this modified engine and its design concept. Then, we report experimental results for thrust, pressure

Received 23 March 2005; revision received 7 June 2005; accepted for publication 15 June 2005.

*Senior Researcher, Project Research Coordination Office, 2-1-1 Sengen, Tsukuba: hiraiwa.tetsuo@jaxa.jp. Member AIAA.
†Subgroup Leader, Combined Propulsion Research Group, 1 Koganezawa, Kimigaya, Kakuda; kanda.takeshi@jaxa.jp. Senior Member AIAA.
‡Researcher, Combined Propulsion Research Group, 1 Koganezawa, Kimigaya, Kakuda; kobayashi.kan@jaxa.jp. Member AIAA.
§Senior Researcher, Combined Propulsion Research Group, 1 Koganezawa, Kimigaya, Kakuda; saito.toshihito@jaxa.jp. Member AIAA.

distributions, and heat flux distributions. We also discuss combustion characteristics of this engine and advantages of the ramp block for the scramjet engine.

II. Engine Model

Figure 1 shows the configuration of the E2R scramjet engine model, and Fig. 2 shows the original configuration of the E2. Total length of each is about 2200 mm, and at the entrance of the inlet, the width and the height of the internal ducts are 200 and 250 mm, respectively. The origin of the x coordinate for the graphs in this paper is at the leading edge of their top wall. The E2 engine was originally a sidewall-compression-type model with a strut, shown in Fig. 2. Its geometrical contraction ratio was 8.33, which was adopted in the E1 engine and yielded sufficient combustion efficiency.[3] Hydrogen fuel was injected from the sidewalls and the strut. Except in its inlet section, this engine had no sweptback angle on its sidewalls. Consequently, the E2 had a longer isolator section, especially for its top wall side of 350 mm, compared with that of 100 mm of the E1 model. The engine was made of copper, and engine components were individually cooled by water.

At the inlet-combustor section, the modified engine model E2R has a new ramp block that fully covers the top wall. The block has two ramps with different angles at its forward section, that is, the inlet and isolator sections. The first ramp has an angle of 7.6 deg to the engine axis. The subsequent second ramp has 14.2 deg. These angles are adopted to prevent separation at the leading edges of each ramp.[6] This two-staged compression system is adopted by restriction of the length of the original inlet of the E2 model. A shock wave generated by the second ramp is designed to impinge on the leading section of the cowl. However, to prevent creation of a strong pressure gradient on the cowl, the shock from the first ramp is designed to not impinge on the cowl. The geometrical contraction ratio is 7.94 for the E2R. These ramp blocks are not actively cooled by water.

From the combustor section to the exit of the E2R, the ramp block has a steady slope of 9 deg. This angle was selected to produce sufficient pressure on the slope and reduce divergence loss of the exhaust flow. Though a smaller angle could not be adopted because of insufficient length of the existing duct from the constant area combustor to the nozzle sections, the angle is smaller than the reattachment angle of a supersonic flow at a backward-facing step, about 18 deg (Refs. 7 and 8). The ramp block used in the E1 had a steeper slope of 45 deg at its tail, also due to installation restrictions.[4] This steeper slope did not produce sufficient pressure on the base area of the ramp block.

On the sidewalls and the ramp block in the combustor section, there are backward-facing steps 4 mm in height for flame-holding. Downstream of these steps, the E2R has three sets of fuel injection holes, as shown in Fig. 1.

1) MV1: the set of the holes is 16 mm downstream of the step on each sidewall. There are six injection holes in total, that is, three on each sidewall.

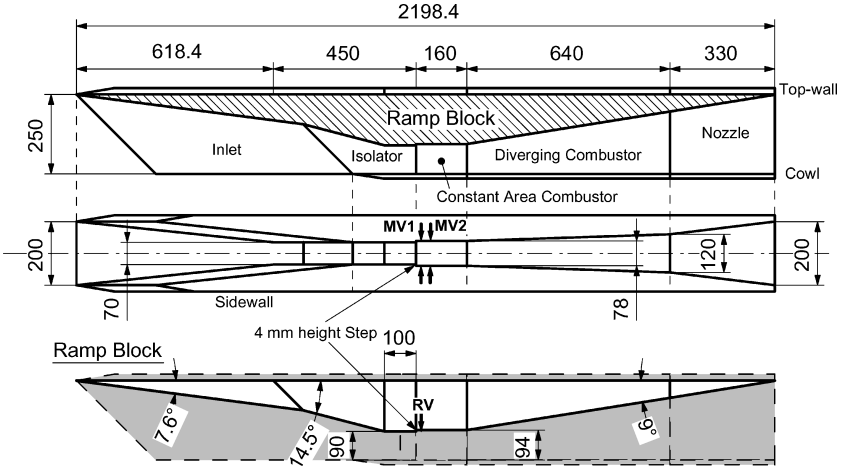

Fig. 1 E2R engine configuration, dimensions in millimeters.

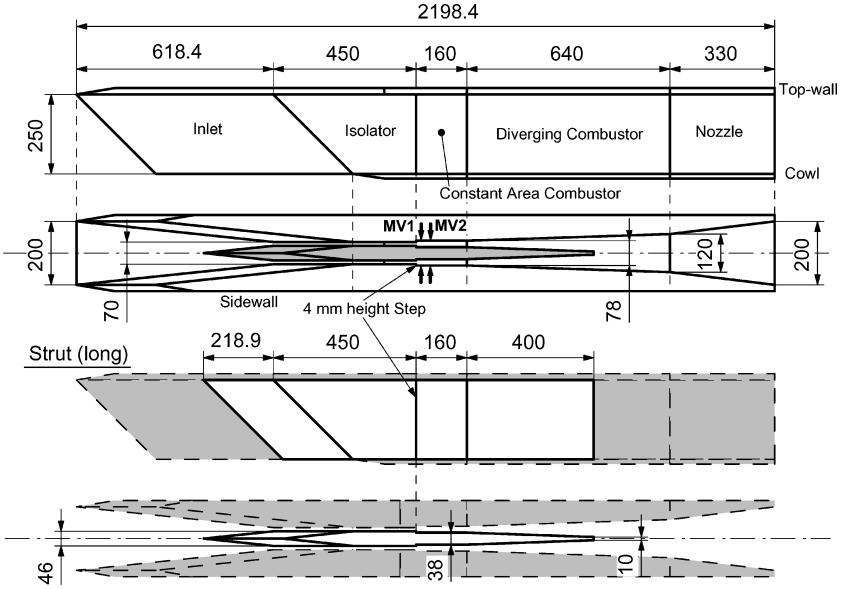

Fig. 2 E2 engine configuration, dimensions in millimeters.

2) MV2: the set is same as MV1, but 30 mm downstream of the step.

3) RV: the set of three injection holes is on the ramp block, 16 mm downstream of the step.

The diameter of each injection hole is 1.5 mm. All of the injection holes supply fuel vertical to the engine wall. In this series of experiments, these holes inject fuel individually or simultaneously. Because the total temperature of the incoming airflow is much higher than the autoignition temperature of hydrogen, there is no igniter in this engine.

III. Experimental Conditions

All of the experiments were conducted under the Mach 8 flight condition. The inflow Mach number of the air was 6.73, presuming a shock wave from the leading edge of an aerospace plane.[2] The total temperature of the incoming airflow was 2400 K and total pressure was 10 MPa, which corresponds to a dynamic pressure of 26 kPa. This airflow was heated not only by a storage air heater but also by a vitiated air heater. Therefore, the airflow contained 27% (mole fraction) H_2O. Oxygen concentration was the same as that in standard air. The supersonic facility nozzle had a square exit, 51 by 51 cm. The nominal static pressure at the exit of the nozzle, P_∞, was 1.6 kPa. The airflow flowed into the engine with a boundary layer that developed on the surface of the facility nozzle. The thickness of this boundary layer was 88 mm at the exit of the nozzle, and its displacement thickness was 33 mm (Ref. 9). The mass flow rate of the airflow toward the engines was 1.54 $kg \cdot s^{-1}$, taking into account the displacement thickness of the boundary layer. The air capture ratio of the E2R inlet was 80% and that of the E2 inlet was 74% (Ref. 10). At the stoichiometric condition, mass flow rates of fuel hydrogen were 44 $g \cdot s^{-1}$ for the E2R engine and 40 $g \cdot s^{-1}$ for the E2, respectively.

Wall pressure and wall temperature were measured. In the present study, the wall pressure was nondimensionalized by the nominal static pressure at the exit of the facility nozzle. The measurement error of the nondimensionalized wall pressure was ± 0.2 in the engine nozzle and ± 0.6 in the other components. The wall temperature was measured with a thermocouple buried 1 mm from the inner surface of the model. Gas sampling and pitot pressure measurement were carried out at 21 locations at the exit of the engine model using sampling probes, each with a fine sampling orifice of 0.3 mm (Ref. 11). With the results of the gas sampling measurement and the pitot pressure measurement, distributions of equivalence ratio, mass flux, and combustion efficiency were attained. The uncertainty of the combustion efficiency was ± 0.05, including the uncertainty of measurement systems and the quenching effect in the sampling probe. The uncertainty of the equivalence ratio and that of the pitot pressure were ± 0.03 each.

The engine model was set on a test bed with a force measurement system (FMS) that measured axial force and lift and pitching moment, simultaneously. This system delivered the drag/thrust within an error of ± 50 N. The center of pitching moment was set at $x = 741.43$ mm and $y = 135.8$ mm. In this study, thrust increment ΔF is defined as $F_{xc} - F_{xa}$, an increase of the thrust in the fueled condition from the thrust in the no-fueled condition measured with the FMS. This means that ΔF is the axial force delivered by combustion in the engine.

IV. One-Dimensional Calculation for the E2R

A one-dimensional calculation was conducted to estimate the kinetic energy efficiency of the inlet and the combustion efficiency. The supersonic nozzle flow from the plenum chamber was also simulated. The calculation procedure was as follows.

1) The temperature of the vitiated air and the flow rates of the air, hydrogen and, oxygen to the vitiation heater were specified. The total pressure was calculated from the choking condition at the facility nozzle. The throat was square, 32.5 by 32.5 mm. The calculated total pressure agreed with the nominal value.

2) The exit size of the facility nozzle was corrected with the measured average displacement thickness of 25 mm (Ref. 9). The vitiated air was assumed to expand isentropically in the nozzle. The calculated Mach number and the static pressure at the nozzle exit agreed with the nominal values.

3) The effect of the swept angle of the engine was ignored, and the distance from the leading edge was used when the calculated results were compared with the experimental data.

4) The air and the combustion gas were assumed to be in the equilibrium condition throughout the engine.

5) The mass capture ratio was 0.80 (Ref. 10).

6) The specified part of the fuel reacted in a stoichiometric condition at the specified location. The ratio of the reacted fuel to the total fuel represented combustion efficiency here. The residual fuel mixed with the residual air. The combustion efficiency was estimated by comparison of the calculated pressure and the measured wall pressure.

7) The combustion gas expanded isentropically in the divergent part of the combustor to the exit of the engine nozzle.

8) The boundary layer was turbulent throughout the engine. The friction coefficient was calculated using the formula of van Driest (see Ref. 12).

10) The inviscid flow condition and the inviscid thrust were calculated first. Next, the friction drag was subtracted from the inviscid thrust, and the net thrust was estimated.

In this calculation method, no heat loss to the engine walls was included because of the difficulty of local heat flux evaluation. With the heat flux data in a similar experimental condition,[4] thrust loss caused by the heat loss was estimated about 10% of the net thrust. This is less than the experimental error of the FMS.

V. Results and Discussion

A. Experimental Thrust Performance

In Fig. 3, the thrust increment of the E2R, ΔF, is plotted against an equivalence ratio ϕ. Open symbols are for the inlet-started condition and closed symbols are for the unstarted condition. Figure 3 also shows ΔF with several fuel-injecting patterns: single-position injection from MV1, MV2, or RV and multiple injection from MV1 + RV or MV1 + MV2. Under the started condition, thrust was proportional to the equivalence ratio from 0.4 to 1. Thereafter, the thrust decreased while the fuel flow rate increased. In this paper, the unstarted condition is defined as this region.

Maximum thrust increment was 500 N at $\phi = 1.05$, that is, $\dot{m}_{\text{fuel}} = 46$ $g \cdot s^{-1}$. Because the internal drag $D_{\text{int}} = 280$ N (Ref. 13), and the cowl drag $D_{\text{cowl}} = 90$ N, the net thrust, $\Delta F - D_{\text{net}} (= D_{\text{int}} + D_{\text{cowl}})$, was 130 N. Therefore, the thrust–drag ratio, $\Delta F / D_{\text{net}}$, was 1.4. This ratio means thrust producing efficiency, that is, a percentage of drag needed to generate a certain thrust. Here, D_{cowl}, the drag on the cowl outer surface, was estimated with shock wave relations and a friction coefficient of 0.0025.

In the E2 engine, the maximum thrust increment was 420 N at $\phi = 1.1$ (Ref. 5). This thrust was only two-thirds of the drag in the airflow condition of 630 N, and no positive net thrust was attained. Although the longer isolator of the E2 engine extended the starting limit at an equivalence ratio greater than the limit of the E1 engine

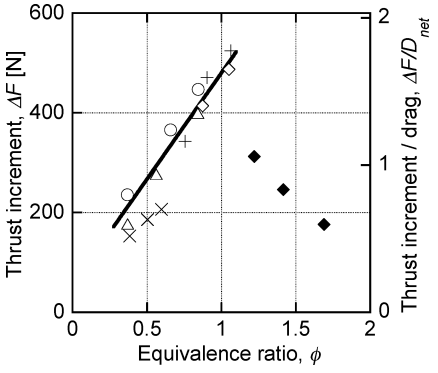

Fig. 3 Thrust increment due to combustion from no-fueled condition: ○, MV1; △, MV2; ◇, MV1 + 2; ×, RV; +, MV1 + RV; ♦, MV1 + 2 unstarted; and ——, linear interpolation.

and the extended limit attained primary combustion around the fuel injectors, it was insufficient to overcome the engine drag. This was caused by insufficient sustenance in the face of the adverse pressure gradient in the isolator and insufficient capture of air at the inlet. The E2R engine had a larger air capture ratio than the E2. Therefore, even at the same equivalence ratio, a greater amount of fuel was injected into the E2R engine. Finally, the thrust increment produced by the E2R engine was greater at 80 N with higher tolerance to an adverse pressure gradient and smaller drag than those of the E2 engine, as shown later in this section.

When the fuel flow rate exceeded $\phi = 1.05$, the E2R fell into the unstarted condition due to separation on the top wall induced by the adverse pressure gradient in the isolator section. In Fig. 3, a gentle decrease of thrust is shown to progress the unstarted condition. While ϕ increased from 1.2 to 1.7, thrust decreased gradually from 320 to 80 N. For our former strut-compression models of the E1 and E2 except the modified model E1SR, the limit of the started condition was clearly found as their thrust decreased promptly. This rapid decrease in thrust was a consequence of a sudden, entire separation of the boundary layer from the inlet top wall. The burnt gas was occasionally seen in the inlet section during the unstarted condition. However, in the case for the E2R, no such flame was observed.

B. Pressure Profiles of E2R in Started Condition

Typical pressure distributions on the ramp and sidewall of the E2R engine are plotted in Fig. 4. A set of profiles of the no-fueled injection case, that is, the case with only the airflow in the engine duct, and three sets with fuel-injection at $\phi = 0.37$, 0.66, and 1.05 are shown in Fig. 4. All of the pressure data are normalized with the wall pressure at the exit of the facility nozzle, P_s, of 1.6 kPa.

Under the no-fueled condition, there was a gradual 15-fold increase in wall pressure from the inlet to the isolator section on both walls. The pressure dropping on both walls at $x = 950$ mm was caused by change of the airflow direction at the second ramp-isolator corner. The highest pressure point on the ramp wall was at $x = 1200$ mm, where the shock wave from the cowl leading edge impinged on the wall. From the divergent combustor to the nozzle section, the flow expanded gradually along slopes of the ramp and sidewalls.

As the fuel flow rate increased, pressure in the combustor section increased. As the combustor pressure increased, pressure in the diverging combustor and the nozzle section, where the thrust was mainly produced, also increased. This pressure increment in the combustor affected the upstream airflow in the isolator. At $\phi = 0.37$, no influence was found at the exit of the second ramp section, $x = 940$ mm. However, in $\phi > 0.37$, the influence by the downstream high pressure was around the downstream side of the ramp, about 100 mm upstream of the step. This local influence on the second ramp is a key to understanding why the E2R can be extended to its starting limit. It will be discussed in a later section.

The engine remained in the started condition until $\phi = 1.05$, and wall pressure recorded its peak of about 75 on the sidewall and 80 at the peak on the top wall. On both walls, the pressure ratios between those peak values and the level at the exit of the inlet section increase to about five times. The E2R engine with the ramp block sustained these high adverse pressure gradients.

C. Combustion Efficiency and One-Dimensional Calculation

Figures 5a and 5b show distributions of the equivalence ratio and the combustion efficiency at the exit of the E2R model based on the pitot pressure measurement and the gas sampling. The local equivalence ratio and combustion efficiency were evaluated from the captured gas mixture, that is, amounts of remaining nitrogen, oxygen, and hydrogen.[11] The overall equivalence ratio of fuel injected from MV1 was 0.85. The local equivalence ratios were about 0.6–0.8 around the top wall. The ratios were lower around the cowl surface. Local combustion efficiencies were greater than 0.8 at most points. In the region with lower equivalence ratio, combustion efficiency was higher.

In the one–dimensional calculation mentioned in Sec. IV, the kinetic energy efficiency of the inlet was 0.98, the equivalence ratio was 1.05, and the combustion efficiency was 0.65. This computational result is plotted in Fig. 6 with the measured wall pressure when the fuel was injected from MV1 and MV2. The pressure levels in the inlet reasonably agreed. Because the calculation model

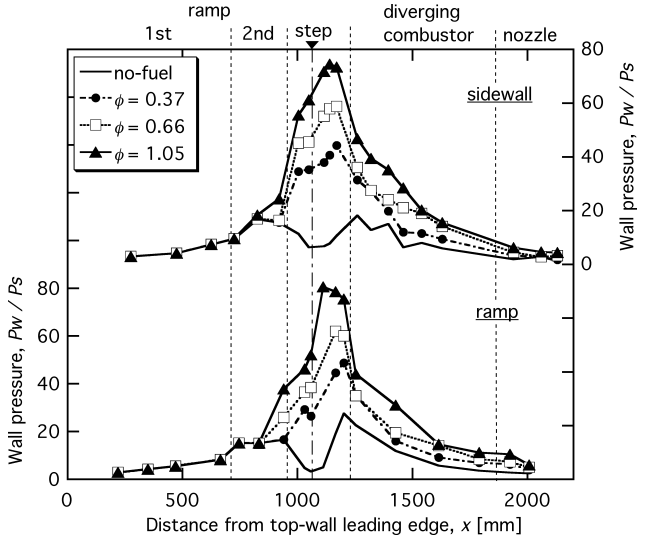

Fig. 4 Typical pressure distributions on the ramp and sidewall of E2R engine.

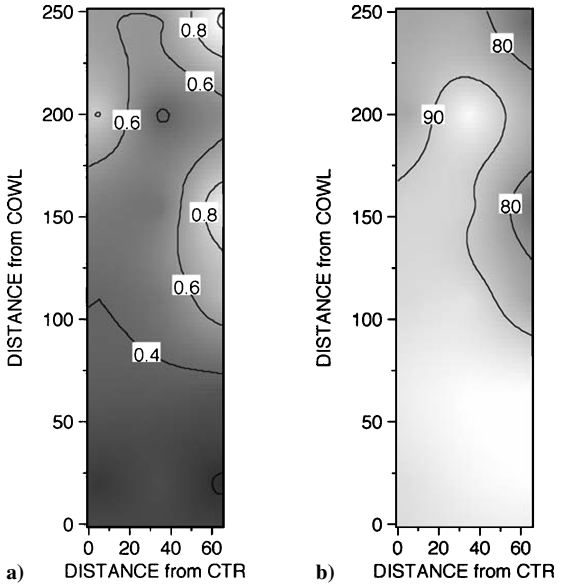

Fig. 5 Cross-sectional distributions of a) equivalence ratio and b) combustion efficiency, %, at E2R engine exit.

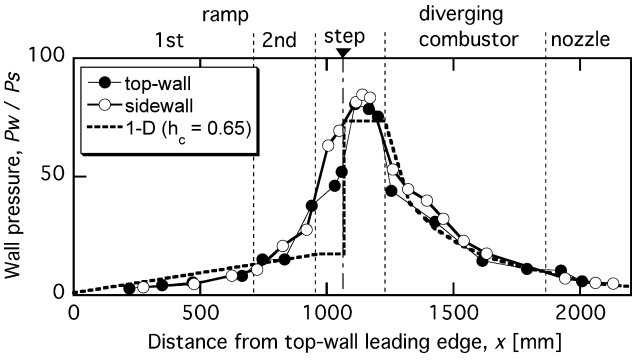

Fig. 6 One-dimensional calculation result for E2R engine.

could not simulate a shock structure, the calculated pressure level in the isolator was lower than the measured one. However, the pressure level at the exit of the combustor agreed with the experimental data. Because an isentropic expansion was presumed in the divergent duct, the level of the pressure was higher than the measured one.

The thrust increment was estimated to be 540 N. This value was 40 N higher than the measured one due to the higher level of calculated pressure in the divergent duct.

D. Comparison of Pressure Profiles in E2R and E2

In this section, wall pressure profiles of the E2R and the E2 models are compared to identify their characteristics. Figure 7 shows their four profiles in no-fueled and fuel-injected conditions. The data of the E2 are from Ref. 5. The equivalence ratios are $\phi = 0.85$ for the E2R and 0.91 for the E2 model, respectively. The E2 model fell into the unstarted condition as ϕ increased from 0.91 to 1.09.

Under the no-fueled condition, both engine's profiles on the sidewall were similar except for a peak at $x = 710$ mm where a shock wave from the strut leading edge impinged in the E2 engine. With fuel injection, both pressure patterns became quite different. On the top wall, this difference is clearly found. At the center of the engines, the E2R generated higher pressure profiles than the E2 model on both walls. Around these stoichiometric conditions, the E2R model produced a thrust approximately 50 N greater than that produced by the E2, which was about one-third of the net thrust.

On the sidewall and the ramp block, the E2R sustained a pressure ratio of 1:6 between its inlet exit and combustor sections. The E2 model sustained a pressure ratio of only 1:1.7 on the top wall. This means that the E2 model had less durability against the adverse pressure gradient on the top wall. Therefore, the limit of its starting condition is $\phi = 0.91$. On the other hand, in the E2R, the boundary layer remained attached to the top wall ramp up to $\phi = 1.05$, even though a small pressure increase appeared at the downstream side of its second ramp.

To clarify the effect of the method of compression on the boundary-layer thickness on the top wall and the effect of the shock waves on it, another one-dimensional calculation was conducted. Figure 8 shows a schematic diagram of this one-dimensional model for the ramp-compression and sidewall-compression inlets. In the calculation, it is assumed that all of the air flowing into the inlet was captured. The effect of the boundary layer was neglected, except for that on the top wall or the ramp block where friction acted. In the ramp-compression model, the height of the duct decreased from 250 to 24 mm. In the sidewall-compression model, the height of the duct did not change, whereas the width of the duct decreased from 200 to 30 mm. The contraction ratios were 7.94 for the ramp-compression model and 8.33 for the sidewall-compression model, respectively. Primary flow was compressed isentropically and was one dimensional, whereas pressure in the boundary layer was the same as that at the edge of the layer. Mass and total energy were conserved. Pressure drag from the sidewall or the ramp was calculated from the pressure of the primary flow. The height of the inflow boundary layer was 0.35, normalized by the height of the inlet at the entrance. Its normalized displacement thickness was 0.131, according to the measurement.[10]

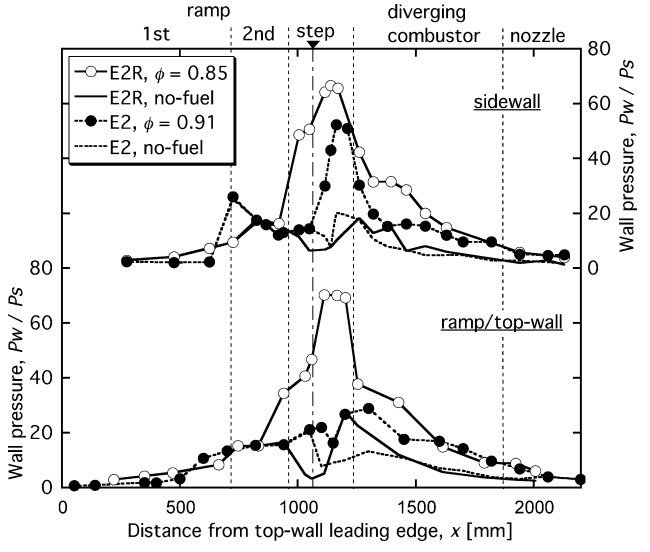

Fig. 7 Comparison of pressure profiles for E2R and E2 engines.

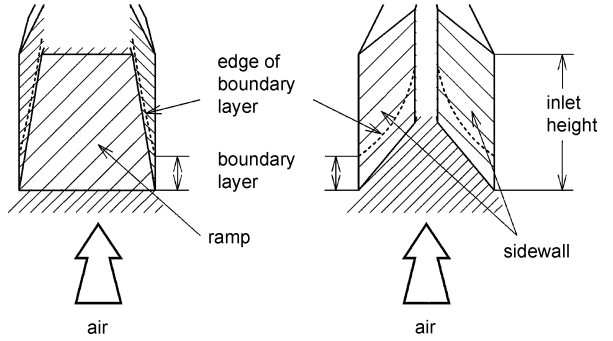

Fig. 8 One-dimensional model for ramp-compression and sidewall-compression inlets.

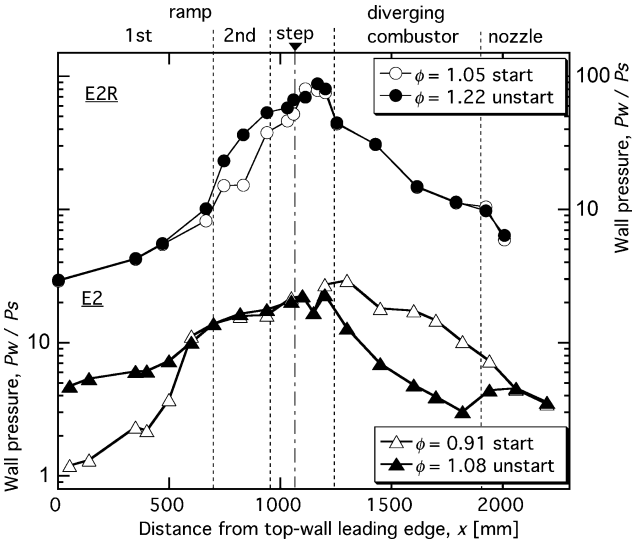

Fig. 9 Pressure profiles of E2R engine under started, $\phi = 1.05$, and unstarted, $\phi = 1.22$, conditions.

The normalized height of the boundary layer at the exit of the inlet was 0.044 in the ramp-compression model and 0.36 in the sidewall-compression model. The difference is caused by the change in inlet width of the top wall or the ramp block, on which the boundary layer grows. Therefore, the increase in downstream pressure has less effect on the flowfield in the ramp-compression inlet than in the sidewall-compression inlet.

E. Pressure Profile Comparisons in Started and Unstarted Conditions

When hydrogen was injected into the engine at a ϕ of more than 1.1, the E2R went into the unstarted condition. As already mentioned, the unstarted condition was defined as the situation in which the thrust declined while the fuel flow rate increased. In Fig. 9, pressure profiles of the E2R under the started, $\phi = 1.05$, and the unstarted, $\phi = 1.22$, conditions are compared. Two profiles of the E2, one with $\phi = 0.91$ and the other with $\phi = 1.08$, are also plotted.

For the E2R model, pressure profiles from the divergent combustor to the nozzle were identical. Only from the second ramp of the inlet to the combustor section, from $x = 600$ to 1100 mm, did the pressure measured at $\phi = 1.22$ become larger than that at

$\phi = 1.05$. This pressure increase at the forward section increased the engine drag. However, because profiles under the started and unstarted conditions were the same in their downstream section, the E2R was still able to keep delivering positive thrust even in the unstarted condition. Therefore, as shown in Fig. 3, the thrust of the E2R model decreased gradually in the condition from $\phi = 1.05$ to 1.22. On the other hand, for the E2 model, profiles in both situations were quite different. Under the started condition, pressure steeply increased at a point of $x = 600$ mm caused by the shock wave from the strut and maintained a sufficient pressure level even in the diverging combustor section. When the engine was in the unstarted condition, pressure from the combustor to the nozzle sections decreased by more than half and pressure in the inlet section doubled or tripled. These changes in wall pressure profile reduced thrust of the E2 model abruptly.

F. Comparison Between MV1, MV2, and RV Injections

Figure 3 also shows that thrust produced by the E2R does not depend on fuel injection positions. In this section, the wall pressure profiles with MV1 and MV2 injections are compared with each other. Side and ramp wall profiles at $\phi = 0.37$ are plotted in Fig. 10. Figure 10 also includes the profiles with RV injection (single and multiple) at $\phi = 0.41$ and 0.65.

On both walls, pressure profiles with MV1 and MV2 injections were identical. Pressure peaks were found at the same place in the combustor section on both walls. With the single RV injection, pressure peaks were also found in the same location, but their peak values were lower than those found in the profiles with MV1 or MV2 injections. These differences in the peak pressure were small in Fig. 10, but pressure integration on the walls showed the difference in their thrusts. With MV injections, thrust of 100 N was produced in the divergent combustor section and thrust of 65 N was produced at the step. With single RV injection, 75 and 50 N were produced. Consequently, as shown in Fig. 3, thrust with the single RV injection measured by FMS was about 40 N lower than thrust with MV1 or MV2 injection.

In Fig. 10, two profiles, a single injection from MV and the multiple injection from MV and RV, are plotted. They are both for $\phi = 0.66$ for the single injection and 0.65 for the multiple injection, which consists of 0.21 from MV1 and 0.44 from RV. Their profiles are almost the same, especially on the tail side. This similarity can be found in Fig. 3, which shows that their thrust increases were 330 N for MV1 only and 300 N for MV1 and RV. These results indicate that combustion and thrust do not have a strong relation to the fuel flow rate from the sidewall in the case with multiple injection.

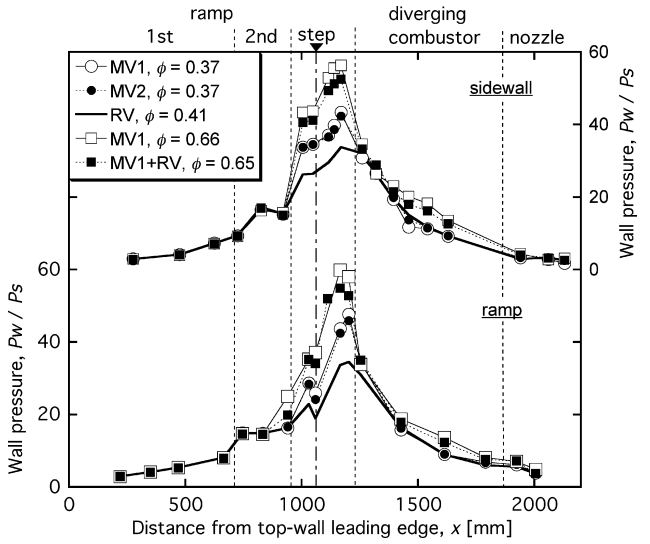

Fig. 10 Pressure profile comparison between MV1, MV2, RV, and multiple injection.

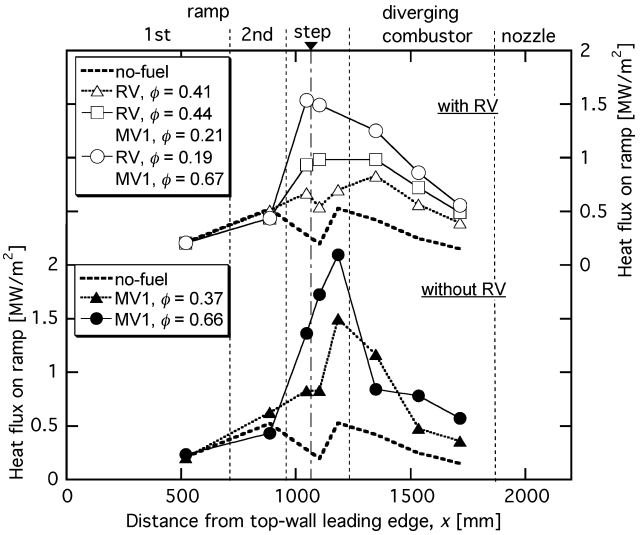

Fig. 11 Typical heat flux profiles with MV1 and RV injections.

G. Heat Flux

Heat flux to the engine walls is important information for evaluating requirements for the active wall-cooling system. Local heat flux was measured by the heat-sink method with thermocouples implanted in the ramp walls.[14] Because the ramp block was not cooled actively, a temperature gradient provided by thermocouples mounted in the block was proportional to the local heat flux to the block. The ramp wall was made of a copper slab with a thickness of 20 mm. In Fig. 11, typical heat flux profiles are compared for cases with or without fuel injection from the RV injector. With single RV injection at $\phi = 0.41$, heat flux at the combustor section around the step was from 0.6 to 0.8 $\mathrm{MW \cdot m^{-2}}$. Coupled with the MV injection at $\phi = 0.44$ from MV1 and 0.21 from RV, measurement showed that heat flux almost doubled there. This feature is the same as that of the wall pressure profiles in Fig. 10, for $x = 1200$ mm. Maximum heat flux of 2.2 $\mathrm{MW \cdot m^{-2}}$ was measured at $x = 1200$ mm with the single MV injection at $\phi = 0.66$.

As shown in the upper part of Fig. 11, multiple RV injections, result in the heat flux to the ramp being lower than that with single MV1 injection. Heat flux with MV1 + RV injections became lower than 1.0 $\mathrm{MW \cdot m^{-2}}$ on the ramp wall in the profile at $\phi = 0.21$ from MV1 and 0.44 from RV. Thrusts in these cases were 330 N for MV1-only injection and 300 N for MV1 + RV injection, as shown in Fig. 10. Moreover, from the profile at $\phi = 0.86$ ($\phi = 0.67$ from MV1 and $\phi = 0.19$ from RV), the heat flux in the combustor section was about 30% lower than that with single MV1 injection, $\phi = 0.66$, although the thrust increased proportionally to the fuel flow rate as shown in Fig. 3. From these results, it is concluded that RV injection can be used to reduce the heat flux to the combustor section with only a slight decrease of the engine thrust.

VI. Conclusions

A subscale scramjet engine model was tested under the Mach 8 flight condition. The model was initially designed to be a sidewall-compression-type engine. In the present tests, it was redesigned to be an engine with ramp and sidewall compressions and with a ramp block installed on the original top wall. The block consisted of two ramps in the inlet and a ramp in the divergent section that covered the entire top wall. Fuel was injected perpendicular to the wall from the sidewalls and the ramp. In the tests, thrust, wall pressure, and wall temperature were measured. From this series of experimental work, the following major conclusions were derived.

1) The E2R model produced larger thrust than its drag at $\phi > 0.6$. This engine showed a thrust profile linear to its fuel flow rate within the started condition.

2) The engine remained in the started condition until $\phi = 1.05$. In the unstarted condition from $\phi = 1.2$ to 1.7, the engine gradually lost its thrust, because the airflow separated gradually from the exit of the inlet.

3) Maximum heat flux to the ramp block, 2.2 $MW \cdot m^{-2}$, was measured in the combustor section when fuel was injected from the sidewalls. Combustion of fuel injected from the sidewalls was dominant.

Acknowledgment

The authors thank the members of the combined engine propulsion research group of the Japan Aerospace Exploration Agency for their cooperation in testing, data processing, and discussion.

References

[1]McClinton, C. R., Rausch, V. L., Nguyen, L. T., and Sitz, J. R., "Preliminary X-43 Flight Test Results," 55th International Astronautical Congress, Paper IAC 04-V.6.01, Oct. 2004.

[2]Chinzei, N., "Research Activities on Scramjets at NAL-KRC in Japan," 15th International Symposium on Air Breathing Engines, Paper ISABE 2001-1075, Sept. 2001.

[3]Kanda, T., Sunami, T., Tomioka, S., Tani, K., and Mitani, T., "Mach 8 Testing of a Scramjet Engine Model," *Journal of Propulsion and Power*, Vol. 17, No. 1, 2001, pp. 132–138.

[4]Kanda, T., Tani, K., Kobayashi, K., Saito, S., and Sunami, T., "Mach 8 Testing of a Scramjet Engine with Ramp Compression," *Journal of Propulsion and Power*, Vol. 18, No. 2, 2002, pp. 417–423.

[5]Kobayashi, K., Tomioka, S., Kanda, T., Tani, K., Hiraiwa, T., and Saito, T., "Modified Water-Cooled Scramjet Engine Tested under M8 Condition," AIAA Paper 2001-3202, July 2001.

[6]Mager, A., "On the Model of the Free, Shock-Separated Turbulent Boundary Layer," *Journal of the Aeronautical Sciences*, Vol. 23, No. 2, 1956, pp. 182–184.

[7]Lamb, J. P., and Oberkampf, W. L., "Review and Development of Base Pressure and Base Heating Correlations in Supersonic Flow," *Journal of Spacecraft and Rockets*, Vol. 32, No. 1, 1995, pp. 8–23.

[8]Roshko, A., and Thomke, G. J., "Observations of Turbulent Reattachment Behind an Axisymmetric Downstream-Facing Step in Supersonic Flow," *AIAA Journal*, Vol. 4, No. 6, 1966, pp. 975–980.

[9]Hiraiwa, T., Mitani, T., Izumikawa, M., and Ono, F., "Calibration Studies of Nozzle Flow in Ramjet Engine Test Facility," 20th International Symposium on Space Technology and Science, Paper 96-d-14, Japan Society for Aeronautical and Space Sciences, May 1996.

[10]Kanda, T., Hiraiwa, T., Izumikawa, M., and Mitani, T., "Experimental Evaluation of Mass Capture Ratio of Scramjet Inlets," *Journal of Propulsion and Power*, Vol. 20, No. 2, 2004, pp. 378–380.

[11]Mitani, T., Takahashi, M., Tomioka, S., Hiraiwa, T., and Tani, K., "Analyses and Application of Gas Sampling to Scramjet Engine Testing," *Journal of Propulsion and Power*, Vol. 15, No. 4, 1999, pp. 572–577.

[12]White, F. M., *Viscous Fluid Flow*, McGraw–Hill, New York, 1974, pp. 632–640.

[13]Mitani, T., Hiraiwa, T., Tarukawa, Y., and Masuya, G., "Drag and Total Pressure Distributions in Scramjet Engines at Mach 8 Flight," *Journal of Propulsion and Power*, Vol. 18, No. 4, 2002, pp. 953–960.

[14]Hiraiwa, T., Sato, S., Tomioka, S., Kanda, T., Shimura, T., and Mitani, T., "Testing of a Scramjet Engine Model in Mach 6 Vitiated Air Flow," AIAA Paper 97-0292, Jan. 1997.